

The dependence of persistent phosphorescence on annealing temperatures in $\text{CaTiO}_3:\text{Pr}^{3+}$ nanoparticles prepared by a coprecipitation technique

Xianmin Zhang^{a,b}, Jiahua Zhang^{a,*}, Xinguang Ren^a, Xiao-Jun Wang^{a,c}

^aKey Laboratory of Excited State Processes, Changchun Institute of Optics, Fine Mechanics and Physics, Chinese Academy of Sciences, 16 Eastern South Lake Road, Changchun 130033, China

^bGraduate School of Chinese Academy of Sciences, Beijing 100039, China

^cDepartment of Physics, Georgia Southern University, Statesboro, GA 30460, USA

Received 9 October 2007; received in revised form 16 November 2007; accepted 18 November 2007
Available online 24 November 2007

Abstract

Red emitting phosphors of $\text{CaTiO}_3:\text{Pr}^{3+}$ nanoparticles with size ranging from 6 to 95 nm have been prepared by a coprecipitation technique and structurally characterized by X-ray diffraction, energy dispersive spectroscopy and scanning electron microscopy. The fluorescence and phosphorescence of $\text{CaTiO}_3:\text{Pr}^{3+}$ nanoparticles as a function of annealing temperature are investigated. It is found that fluorescence intensities monotonously increase with increasing temperature. However, a maximum in phosphorescence with the increase of annealing temperature occurs for the sample prepared at 700 °C. Based on the measurement of fluorescence emission, fluorescence excitation and reflectance spectra as well as time decay patterns of fluorescence and phosphorescence, it is demonstrated that the dependence of fluorescence and phosphorescence on annealing temperature originates from the decrease of surface defects with the increase of temperature.

© 2007 Elsevier Inc. All rights reserved.

Keywords: Photoluminescence; Phosphorescence; CaTiO_3 ; Pr^{3+} ; Nanoparticle

1. Introduction

It is well known that reduction of the particle size in a crystalline system can result in remarkable modifications of properties differing from those of the bulk, which mainly come from the high surface-to-volume ratio and the quantum confinement effect of nanomaterials. Rare earth (RE)-doped phosphors have been intensively applied in luminescent and display devices [1,2]. In 1994, Bhargava et al. [3] reported that the radiative transition rate of $\text{ZnS}:\text{Mn}$ nanocrystals increased 5-fold in comparison with that of the bulk. Despite the fact that this result was strongly criticized later, studies on the fluorescence (light emission from the materials while it is irradiated by light) properties of RE-doped nanophosphors, such as electronic

transitions [4–6], confinement on energy transfer [7,8], and surface effects [9–12], have attracted great interest. Among these properties, surface defects have attracted intensive attention as a major factor affecting the fluorescence efficiency of nanosized phosphors. Generally, surface defects are regarded as a bad factor to the nanophosphors because they quench the luminescence efficiency of conventional phosphors [9]. Nevertheless, in phosphorescence (light emission that persists after the cessation of excitation) materials, defects acting as traps of energy storage benefit phosphorescence emission [13–17]. To improve the phosphorescence intensity and persistent time, the increase of density of traps in these materials is needed [18]. The surface defects might act as traps that are beneficial for the generation of phosphorescence when they are adjusted in suitable depth. However, at present, it is insufficient to study the effect of surface defects on phosphorescence.

*Corresponding author. Fax: +86 431 8617 6317.

E-mail address: zjiahua@public.cc.jl.cn (J. Zhang).

Pr^{3+} -doped CaTiO_3 phosphors have attracted intense interest to meet the challenge of achieving of intense red-emitting phosphors in the field of display and lighting technologies [19,20]. The single emission peaking at 610 nm originates from the intra- $4f \ ^1D_2 \rightarrow \ ^3H_4$ transition of Pr^{3+} with the chromaticity coordinates at $x=0.680$ and $y=0.311$, which is very close to the coordinates of the ‘ideal red’ [21]. Moreover, as an oxide phosphor, $\text{CaTiO}_3:\text{Pr}^{3+}$ has better physical and chemical stabilities than that of the conventional sulfide phosphors [22]. To investigate the optical properties of nanosized $\text{CaTiO}_3:\text{Pr}^{3+}$ phosphors or thin films, many preparation methods have been used, such as sol-gel process [23–26], radio frequency sputtering [27], and spray pyrolysis [28]. To the best of knowledge, no studies have been reported on the preparation of $\text{CaTiO}_3:\text{Pr}^{3+}$ nanoparticles using a coprecipitation technique. In previous studies, the emphasis of the investigation was on the fluorescence property. It is found that the fluorescence intensity reduces in $\text{CaTiO}_3:\text{Pr}^{3+}$ nanoparticles due to the increase of surface defects as nonradiative transition centers [23–26]. However, little work has been done to study the effect of surface defects on phosphorescence, although it has been observed [23]. Recently, we found that some surface defects acting as traps of energy storage contribute to the phosphorescence in $\text{CaTiO}_3:\text{Pr}^{3+}$ nanoparticles prepared by an improved sol gel technique [29]. It is significant to study the effect of surface defects on fluorescence and phosphorescence, and further manipulate them to design novel luminescent materials.

In this paper, $\text{CaTiO}_3:\text{Pr}^{3+}$ nanoparticles have been prepared by a coprecipitation technique. The temperature dependence of fluorescence and phosphorescence in $\text{CaTiO}_3:\text{Pr}^{3+}$ nanoparticles is investigated. It is found that fluorescence intensities monotonously increase with increasing temperature. However, a maximum in phosphorescence with the increase of annealing temperature occurs for the sample prepared at 700 °C. The dependence of fluorescence and phosphorescence on the decrease of surface defects with the increase of annealing temperature is discussed by measuring fluorescence (photoluminescence, photoluminescence excitation) and reflectance spectra as well as time decay patterns of fluorescence and phosphorescence.

2. Experimental section

$\text{Ca}(\text{NO}_3)_2 \cdot 4\text{H}_2\text{O}$ (99.99%) 0.03 M and PrCl_3 solution (Pr_6O_{11} was dissolved in HCl, the concentration of PrCl_3 is 2.82 mg/ml) were first dissolved in the ethanol and NH_3OH solution (pH = 12). Under constant magnetic stirring, 0.03 M $\text{Ti}(\text{OC}_4\text{H}_9)_4$ was added in a dropwise manner. To reduce the hydrolytic rate of $\text{Ti}(\text{OC}_4\text{H}_9)_4$, the solution was kept around 0 °C by an ice-water mixture all the time. After stirring for 10 min, the solution was then precipitated for 10 h. The precipitate was collected by centrifuge, washed several times using distilled water and then dried

at 65 °C under vacuum. $\text{CaTiO}_3:\text{Pr}^{3+}$ nanoparticles were obtained after annealing the as-prepared sample in air. The bulk powder was synthesized by conventional solid-state reaction at 1400 °C for 3 h in air.

The structural characterization was analyzed by X-ray diffraction (XRD; Rigaku D/max-rA) spectra with the $\text{CuK}\alpha$ line of 1.540 78 Å. The morphology of products was observed by field emission scanning electron microscopy (FESEM, Hitachi S-4800). Energy-dispersive spectroscopy (EDS) was performed on a GENESIS2000XMS 60S (EDAX Inc). Fluorescence emission and excitation spectra as well as phosphorescence decay curves were measured using a Hitachi F-4500 fluorescence spectrophotometer. Fluorescence and phosphorescence are measured after irradiation by 365 nm ultraviolet (UV) light for 10 min. For lifetime measurement, the third (355 nm) harmonic of an Nd-YAG laser is used as the excitation source, and the signal is detected with a Tektronic digital oscilloscope mode TDS 3052.

3. Results and discussion

3.1. Microstructure character of the $\text{CaTiO}_3:\text{Pr}^{3+}$ nanoparticles: XRD, SEM and EDS studies

Fig. 1 shows the XRD patterns of $\text{CaTiO}_3:\text{Pr}^{3+}$ nanoparticles prepared at various annealing temperatures and a bulk material. The as-prepared sample is amorphous, as shown in Fig. 1a. XRD patterns of nanoparticles (for b–f) are consistent with the phase of bulk, which is orthorhombic CaTiO_3 (JCPDS Card No. 82-0228). Several small peaks from TiO_2 (Δ) and CaO (∇) are also observed, respectively. The XRD peak of $\text{CaTiO}_3:\text{Pr}^{3+}$ nanoparticles is wider and the position shifts to the smaller angle than that of the bulk because of size effect [30]. By applying the

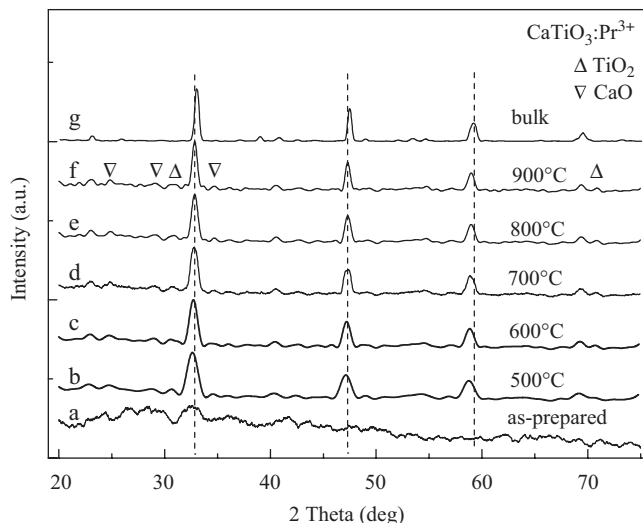


Fig. 1. XRD patterns of $\text{CaTiO}_3:\text{Pr}^{3+}$ nanoparticles obtained at different annealing temperature (a) as-prepared, (b) 500 °C, (c) 600 °C, (d) 700 °C, (e) 800 °C, (f) 900 °C and (g) bulk sample. Several small peaks from TiO_2 (Δ) and CaO (∇) are also observed.

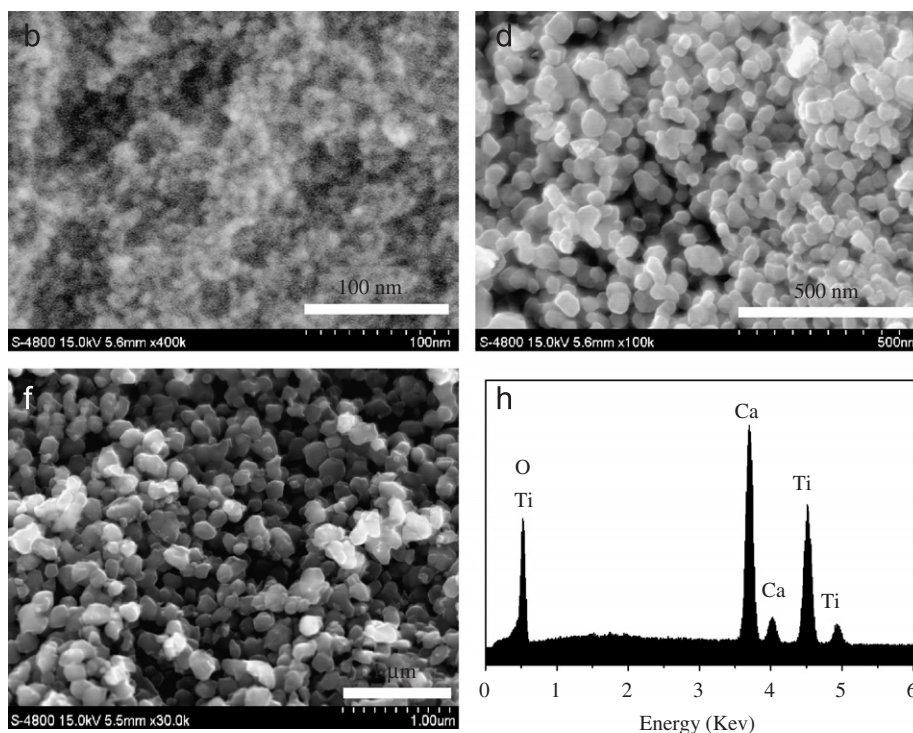


Fig. 2. The representative SEM images of $\text{CaTiO}_3:\text{Pr}^{3+}$ nanoparticles for sample b, d and f. (h) EDS analysis of sample d.

Scherrer formula to the full-width at half-maximum of the diffraction peaks, one can calculate the mean particle sizes of samples b, c, d, e and f to be 6, 11, 42, 63 and 95 nm, respectively, which is consistent with that determined by the representative SEM images of samples b, d and f, as shown in Fig. 2. The analysis of chemical composition of sample d using EDS (Fig. 2d) confirms the results of XRD on the phase composition.

3.2. Temperature dependence of the fluorescence

Fluorescence emission (EM) and excitation (EX) spectra of $\text{CaTiO}_3:\text{Pr}^{3+}$ nanoparticles prepared at various annealing temperatures are presented in Fig. 3, where the curve for bulk powders is also plotted for comparison. The EM spectra show a red emission line at 615 nm, originating from the intra- $4f^1\text{D}_2\text{--}^3\text{H}_4$ transition of Pr^{3+} [21]. The EX spectra monitoring the red emission mainly consists of three broad bands (A–C) in the UV region, which are located at 320 nm (A), 265 nm (B) and 375 nm (C), respectively. In comparison with the spectra of $\text{CaTiO}_3:\text{Pr}^{3+}$ bulk powders (dashed line), band A shifts from 330 nm in the bulk to 320 nm in the nanoparticles. The position of band A is experimentally observed to be consistent with that of the band edge absorption of the CaTiO_3 host [21], indicating that the blue shift of band A in the nanoparticles is the result of size confinement effect [27]. Band B exhibiting no obvious shift in the nanoparticles is attributed to the $4f^2\text{--}4f5d$ absorption of Pr^{3+} ions [21]. Band C originates from a low-lying intervalence charge transfer state ($\text{Pr}^{3+}\text{--Ti}^{4+}$) [31]. The blue shift of the band-edge absorption of CaTiO_3

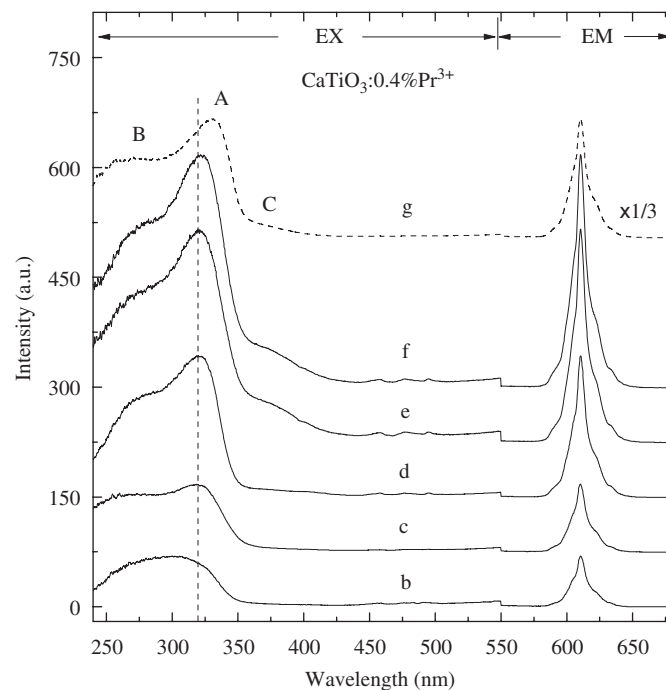


Fig. 3. Fluorescence excitation (EX) and emission (EM) spectra of $\text{CaTiO}_3:\text{Pr}^{3+}$ nanoparticles obtained at different annealing temperature and bulk sample. EM is detected by exciting into the strong absorption band of the host with 320 nm for the nanoparticles and 330 nm for the bulk.

nanoparticles in comparison with that of the bulk is also confirmed with the diffused reflectance spectra, as shown in Fig. 4. A strong absorption edge of the host around 320 nm

for nanoparticles (Fig. 4b–f) and 330 nm (Fig. 4g) for bulk powder is clearly presented, being in good agreement with the position of the corresponding band A observed in PLE

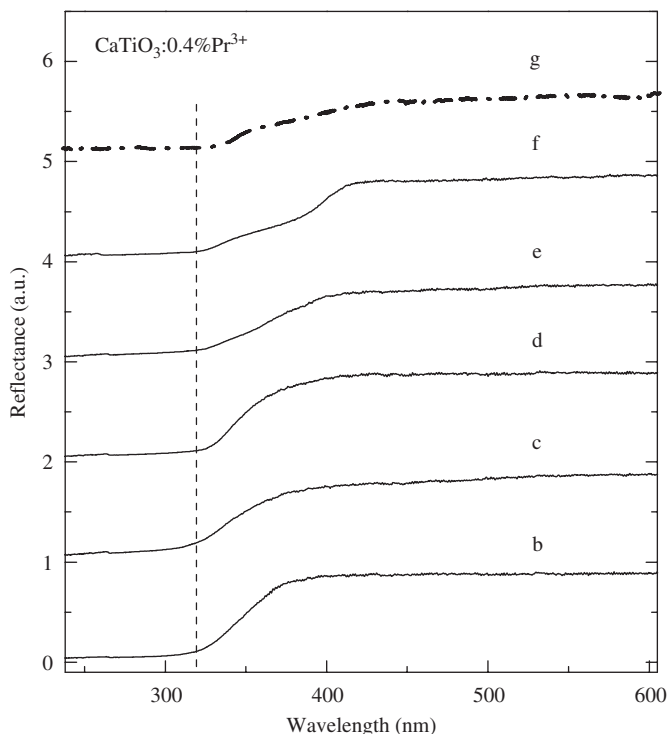


Fig. 4. Diffused reflectance spectra of $\text{CaTiO}_3:\text{Pr}^{3+}$ nanoparticles for samples b–g (bulk powder).

spectra of Fig. 3. It is found that the reflectance of nanoparticles is higher than that of the bulk powders, as shown in Fig. 4, which is due to the decrease of internal bulk defects in $\text{CaTiO}_3:\text{Pr}^{3+}$ nanoparticles. In our previous work [22], Ca and Ti vacancies are mainly crystal defects in bulk $\text{CaTiO}_3:\text{Pr}^{3+}$ phosphors, which act as nonradiation centers reducing the fluorescence emission efficiency. The absorption in the whole visible range (Ti vacancies) and at around 380 nm (Ca vacancies) reduces the reflectance (around 0.6 at 600 nm) in bulk $\text{CaTiO}_3:\text{Pr}^{3+}$ phosphors. The addition of RE oxides Ln_2O_3 ($\text{Ln} = \text{Lu}, \text{La}, \text{Gd}$) in $\text{CaTiO}_3:\text{Pr}^{3+}$ can reduce these defects because of the substitution for Ca^{2+} or Ti^{4+} by Ln^{3+} . The body color of bulk $\text{CaTiO}_3:\text{Pr}^{3+}$ without Ln_2O_3 addition is brown and becomes nearly white when Ln_2O_3 is added. In this report, the body color of $\text{CaTiO}_3:\text{Pr}^{3+}$ nanoparticles is whitish. This indicates that there are nearly no Ca and Ti vacancies in nanoparticles. Therefore, we deduce that the defects in $\text{CaTiO}_3:\text{Pr}^{3+}$ nanoparticles mainly come from the surface defects rather than from the internal defects.

To further investigate the mechanism of fluorescence intensity dependence on annealing temperature, the lifetimes of the $^1\text{D}_2$ level of Pr^{3+} in CaTiO_3 nanoparticles are measured in room temperature, as shown in Fig. 5(b, d–f). The decay curve can be well fitted as a function of time t by a double exponential equation

$$I(t) = A_1 \exp(-t/\tau_1) + A_2 \exp(-t/\tau_2), \quad (1)$$

where I is the fluorescence intensity, A_1 and A_2 are the amplitudes for each component, and τ_1 and τ_2 are the decay constants for the two components, respectively.

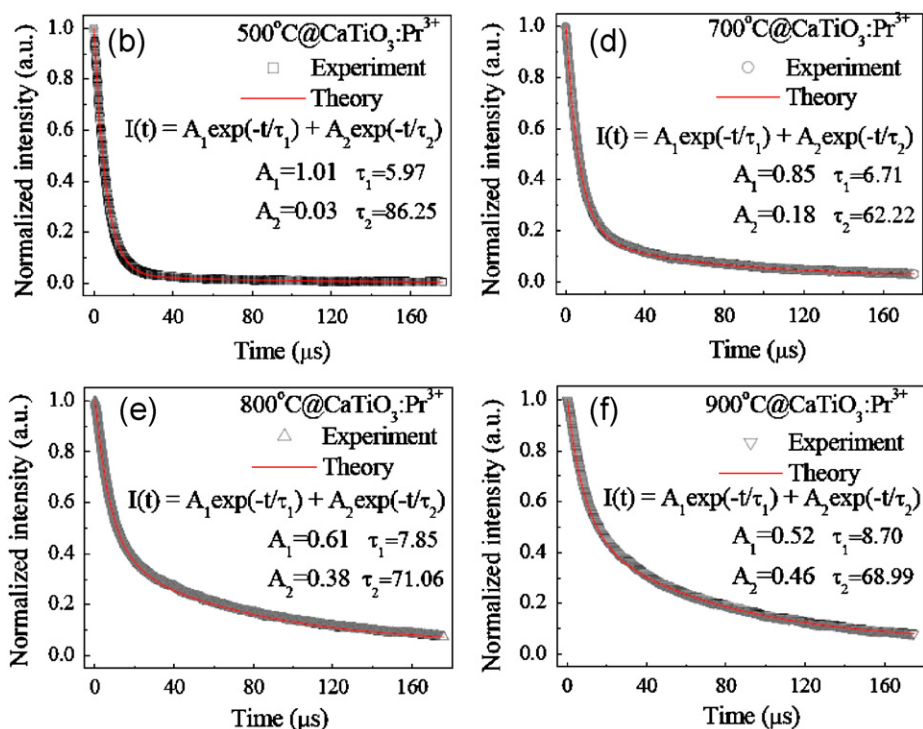


Fig. 5. Fluorescence lifetime of Pr^{3+} ($^1\text{D}_2\text{-}^3\text{H}_4$) in $\text{CaTiO}_3:\text{Pr}^{3+}$ nanoparticles for samples b, d, e, and f.

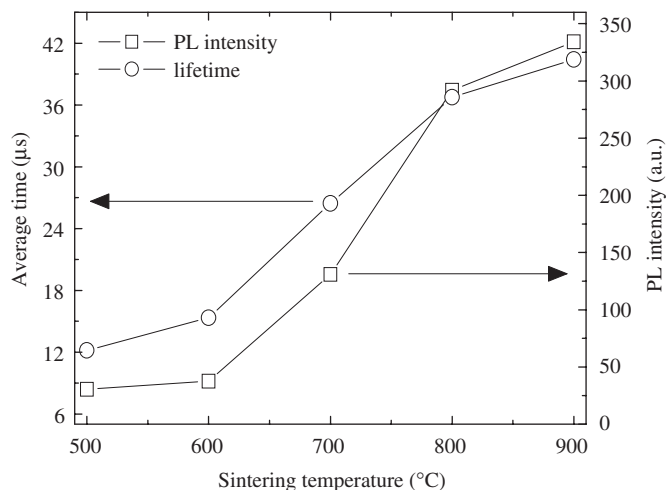


Fig. 6. Dependence of the lifetimes of the 1D_2 level and the fluorescence intensities of red emission ($\lambda_{ex} = 320$ nm) on annealing temperature.

The average lifetime for Pr^{3+} can be determined by the formula [32]

$$\tau = (A_1\tau_1^2 + A_2\tau_2^2)/(A_1\tau_1 + A_2\tau_2). \quad (2)$$

According to Eqs. (1) and (2), the dependence of lifetimes (τ) on annealing temperature is plotted in Fig. 6. It is found that the lifetimes become longer with the increase of annealing temperature, showing the enhancement of $^1D_2 \rightarrow ^3H_4$ emission efficiency of Pr^{3+} . For comparison, the dependence of fluorescence EM intensities on annealing temperature is also presented, showing that fluorescence intensities increase with the increase of annealing temperature in the same scale as the increase of lifetimes of $^1D_2 \rightarrow ^3H_4$ emission efficiency. This indicates that the fluorescence enhancement is due to the increase of the $^1D_2 \rightarrow ^3H_4$ emission efficiency of Pr^{3+} . In nanosized phosphors, the numerous defects on their surfaces due to large surface-to-volume ratio acting as nonradiative centers reduce luminescent efficiency [23–26]. With the increase of preparing temperature, the nonradiative centers reduce because of the decrease of surface defects. Thus, the $^1D_2 \rightarrow ^3H_4$ emission efficiency of Pr^{3+} in $CaTiO_3$ nanoparticles is enhanced with the increase of annealing temperature. In this report, it is assumed that all kinds of surface defects reduce at the same rate with the increase of annealing temperature because they all depend on the surface-to-volume ratio. Therefore, surface defect properties are independent of annealing temperature.

3.3. Temperature dependence of the phosphorescence

Fig. 7 illustrates the time decay curves of phosphorescence in $CaTiO_3:Pr^{3+}$ after irradiation with 365 nm UV light for 10 min. The largest integrated area under the decay curve is experimentally observed for the sample d prepared at 700 °C. Fig. 8 shows the dependence of phosphorescence intensities on preparing temperature.

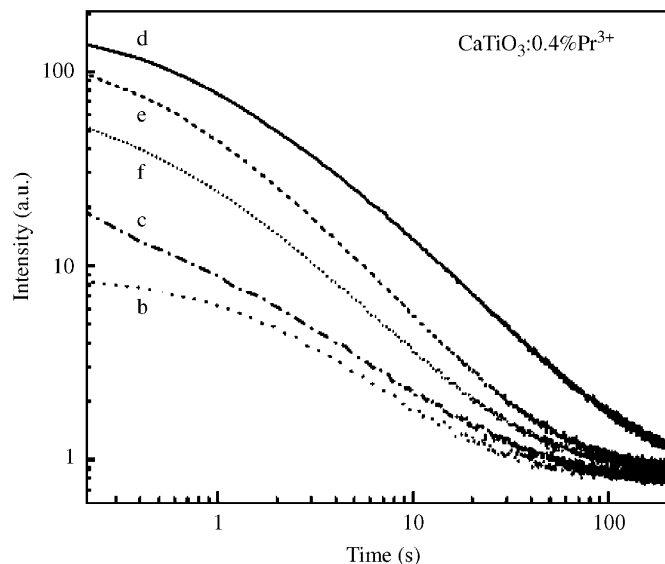


Fig. 7. Phosphorescent decay curves of $CaTiO_3:Pr^{3+}$ nanoparticles for samples b–f after irradiation by 365 nm UV light for 10 min.

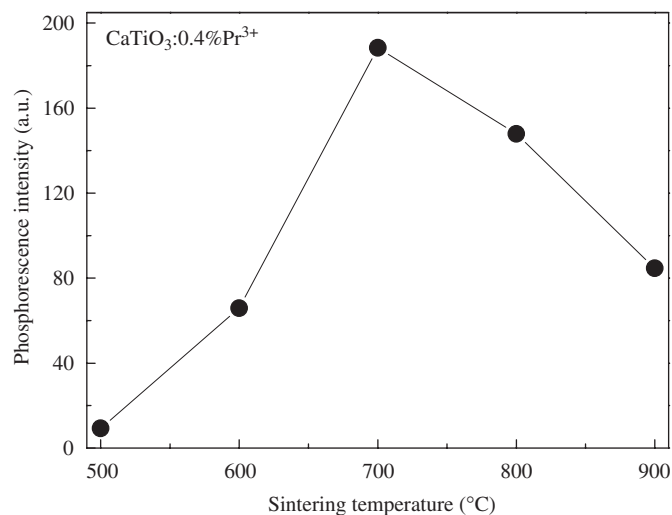


Fig. 8. Dependence of phosphorescence intensities of $CaTiO_3:Pr^{3+}$ on annealing temperature.

The existence of maximum phosphorescence for sample d was demonstrated. In view of some surface defects that can act as traps for phosphorescent emission [29], it is deduced that the appearance of phosphorescent maximum originates from the decrease of surface defects. The phosphorescence intensity is proportional to the number of traps for energy storage and the recombination efficiency of the released carries with luminescent centers. With the increase of annealing temperature, the increase of particle size reduces the number of surface defects on the particles. On the one hand, this reduces the number of traps for energy storage. On the other hand, the transfer efficiency from filled trap to luminescent centers enhances because of the reduction of nonradiative recombination centers. As a result, the maximal phosphorescence intensity with the

increase of annealing temperature occurs at a temperature, which is 700 °C for CaTiO₃:Pr³⁺ nanoparticles.

4. Conclusion

CaTiO₃:Pr³⁺ nanoparticles have been prepared by a coprecipitation technique. It is found that the fluorescence intensities increase with the increase of annealing temperature in the same scale as the increase of lifetimes of ¹D₂–³H₄ emission efficiency. This indicates that the fluorescence enhancement is due to the increase of the ¹D₂–³H₄ emission efficiency of Pr³⁺. With the increase of annealing temperature, the reduction of surface to volume ratio decreases the surface defects acting as nonradiative recombination centers and increases the ¹D₂–³H₄ emission efficiency. The phosphorescence of CaTiO₃:Pr³⁺ nanoparticles depends on the surface defects. With the increase of preparation temperature, the reduction of trap numbers and the enhancement of the recombination efficiency of released carriers lead to the appearance of the maximal phosphorescence for the sample prepared at 700 °C. The work promotes our knowledge about the effect of surface defects on the fluorescence and phosphorescence of nanophosphors.

Acknowledgments

This work is financially supported by the MOST of China (2006CB601104, 2006AA03A138) and the National Natural Science Foundation of China (10574128, 10774141).

References

- [1] G. Blasse, B.C. Grabmaier, *Luminescence Materials*, Springer, Berlin, 1994.
- [2] S. Shionoya, W.M. Yen, *Phosphors Handbook*, CRC Press, New York, 1999.
- [3] R. Bhargava, D. Gallagher, X. Hong, *Phys. Rev. Lett.* 72 (1994) 416.
- [4] R.S. Meltzer, S.P. Feofilov, B.M. Tissue, H.B. Yuan, *Phys. Rev. B.* 60 (1999) 14012.
- [5] R.S. Meltzer, W.M. Yen, H. Zheng, S.P. Feofilov, M.J. Dejneka, *Phys. Rev. B.* 66 (2002) 224202.
- [6] S.F. Wuister, C.M. Donega, A. Meijerink, *Phys. Chem. Chem. Phys.* 6 (2004) 1633.
- [7] G.K. Liu, H.Z. Zhuang, X.Y. Chen, *Nano. Lett.* 2 (2002) 535.
- [8] G.K. Liu, X.Y. Chen, H.Z. Zhuang, S. Li, R.S. Niedbala, *J. Solid. State Chem.* 171 (2003) 123.
- [9] B.M. Tissue, *Chem. Mater.* 10 (1998) 2837.
- [10] D.K. Williams, B. Bihari, B.M. Tissue, J.M. Mchale, *J. Phys. Chem. B.* 102 (1998) 916.
- [11] C.H. Yan, L.D. Sun, C.S. Liao, Y.X. Zhang, Y.Q. Lu, S.H. Huang, S.Z. Lu, *Appl. Phys. Lett.* 82 (2003) 3511.
- [12] O. Lehmann, K. Kompe, M. Haase, *J. Am. Chem. Soc.* 126 (2004) 14935.
- [13] T. Matsuzawa, Y. Aoki, N. Takeuchi, Y. Murayama, *J. Electrochem. Soc.* 143 (1996) 2670.
- [14] J.R. Qiu, A.L. Gaeta, K. Hirao, *Chem. Phys. Lett.* 333 (2001) 236.
- [15] F. Clabau, X. Rocquefelte, S. Jobic, T. Le Mercier, P. Deniard, M.H. Whangbo, A. Garcia, *Chem. Mater.* 17 (2005) 3904.
- [16] F. Clabau, X. Rocquefelte, T. Le Mercier, P. Deniard, S. Jobic, M.H. Whangbo, *Chem. Mater.* 18 (2006) 3212.
- [17] Y.L. Liu, B.F. Lei, C.S. Shi, *Chem. Mater.* 17 (2005) 2108.
- [18] D. Jia, R.S. Meltzer, W.M. Yen, W. Jia, X. Wang, *Appl. Phys. Lett.* 80 (2002) 1535.
- [19] A. Vecht, D.W. Smith, S.S. Chadha, C.S. Gibbons, *J. Vac. Sci. Technol. B* 12 (1994) 781.
- [20] S.H. Cho, J.S. Yoo, J.D. Lee, *J. Electrochem. Soc.* 143 (1996) L231.
- [21] P.T. Diallo, P. Boutinaud, R. Mahiou, J.C. Cousseins, *Phys. Stat. Sol. A* 160 (1997) 255.
- [22] X.M. Zhang, J.H. Zhang, X. Zhang, L. Chen, Y.S. Luo, X.J. Wang, *Chem. Phys. Lett.* 434 (2007) 237.
- [23] Y.X. Pan, Q. Su, H.F. Xu, T.H. Chen, W.K. Ge, C.L. Yang, M.M. Wu, *J. Solid. State. Chem.* 174 (2003) 69.
- [24] E. Pinel, P. Boutinaud, G. Bertrand, C. Caperaa, J. Cellier, R. Mahiou, *J. Alloys Compds.* 374 (2004) 202.
- [25] B. Yan, K. Zhou, *J. Alloys Compds.* 398 (2004) 165.
- [26] X.M. Liu, P.Y. Jia, J. Lin, G.Z. Li, *J. Appl. Phys.* 99 (2006) 124902.
- [27] P. Boutinaud, E. Tomasella, A. Ennajdaoui, R. Mahiou, *Thin Solid Films* 515 (2006) 2316.
- [28] P. Boutinaud, E. Pinel, R. Mahiou, *Opt. Mater.* Available online 19 June 2007.
- [29] X.M. Zhang, J.H. Zhang, Z.G. Nie, M.Y. Wang, X.G. Ren, X.J. Wang, *Appl. Phys. Lett.* 90 (2007) 151911.
- [30] Z.G. Wei, L.D. Sun, C.S. Liao, J.L. Yin, X.C. Jiang, C.H. Yan, *J. Phys. Chem. B.* 106 (2002) 10610.
- [31] P. Boutinaud, E. Pinel, M. Dubois, A.P. Vink, R. Mahiou, *J. Lumin.* 111 (2005) 69.
- [32] T. Fujii, K. Kodaira, O. Kawachi, N. Tanaka, H. Yamashita, M. Anpo, *J. Phys. Chem. B.* 101 (1997) 10631.